Hippo-TAZ signaling is the master regulator of the onset of triple-negative basal-like breast cancers

Soyama, Hirotoshi ; Nishio, Miki ; Ootani, Junji ; Sakuma, Toshiko ; Takao, Shintaro ; Hara, Shigeo ; Masuda, Takaaki ; Mimori, Koshi ;…

(Citation)
Proceedings of the National Academy of Sciences,119(29):e2123134119

(Issue Date)
2022-07-11

(Resource Type)
journal article

(Version)
Version of Record

(URL)
https://hdl.handle.net/20.500.14094/0100476794

PNAS RESEARCH ARTICLE | MEDICAL SCIENCES

Hippo-TAZ signaling is the master regulator of the onset of triple-negative basal-like breast cancers

Hirotoshi Soyama[a,b,1], Miki Nishio[a,1], Junji Otani[a], Toshiko Sakuma[c], Shintaro Takao[d], Shigeo Hara[e], Takaaki Masuda[f], Koshi Mimori[f], Shinya Toyokuni[g], John P. Lydon[h], Kazuwa Nakao[i], Hiroshi Nishina[j], Takumi Fukumoto[b], Tomohiko Maehama[a,2,3], and Akira Suzuki[a,2,3]

Edited by Tak Mak, University of Toronto, Toronto, Canada; received December 24, 2021; accepted April 14, 2022

Breast cancer is the most frequent malignancy in women worldwide. Basal-like breast cancer (BLBC) is the most aggressive form of this disease, and patients have a poor prognosis. Here, we present data suggesting that the Hippo–transcriptional coactivator with PDZ-binding motif (TAZ) pathway is a key driver of BLBC onset and progression. Deletion of *Mob1a/b* in mouse mammary luminal epithelium induced rapid and highly reproducible mammary tumorigenesis that was dependent on TAZ but not yes-associated protein 1 (YAP1). In situ early-stage BLBC-like malignancies developed in mutant animals by 2 wk of age, and invasive BLBC appeared by 4 wk. In a human estrogen receptor^{+} luminal breast cancer cell line, TAZ hyperactivation skewed the features of these luminal cells to the basal phenotype, consistent with the aberrant TAZ activation frequently observed in human precancerous BLBC lesions. TP53 mutation is rare in human precancerous BLBC but frequent in invasive BLBC. Addition of *Trp53* deficiency to our *Mob1a/b*-deficient mouse model enhanced tumor grade and accelerated cancer progression. Our work justifies targeting the Hippo-TAZ pathway as a therapy for human BLBC, and our mouse model represents a powerful tool for evaluating candidate agents.

MOB1 | TAZ | Hippo | triple-negative breast cancer | basal-like breast cancer

Significance

A universal oncogenic driver of basal-like breast cancer (BLBC) has resisted identification. We show that continuous transcriptional coactivator with PDZ-binding motif (TAZ) activation in precancerous murine luminal cells generates luminal cancers that later become BLBCs. Subsequent TP53 alteration, a feature of invasive human BLBCs, accelerates tumor progression. Because BLBC development is inhibited by TAZ inactivation in vivo, our work provides a sound rationale for targeting Hippo-TAZ signaling as therapy for human BLBC. Our mouse model of BLBC represents a powerful tool for evaluating such drugs.

Breast cancer (BC) is the most frequent cancer in women worldwide and remains the second leading cause of death (1). Human BC is a heterogeneous disease that has been classified into various subgroups based on the expression (or not) of the estrogen receptor (ESR), progesterone receptor (PGR), and/or human epidermal growth factor receptor 2 (HER2; ERBB2) (2). Triple-negative BC (TNBC; ESR^{-}PGR^{-}HER2^{-}) is the most complex, aggressive, and fatal subtype of BC, and no targeted therapies currently exist to treat it. TNBC patients invariably develop resistance to existing chemotherapeutic regimens, leading to ∼90% treatment failure and a very low 5-y survival rate (3). Thus, there is a pressing need to better understand TNBC onset and progression mechanisms in order to develop more effective treatments.

In humans and mice, the mammary epithelial cell (MEC) population is composed of the luminal cell and basal cell subsets. Luminal cells line the lumens of the mammary ducts and alveoli and are responsible for the production and transport of milk. Basal cells contact the basement membrane and contract to pump milk through the ducts. The majority of BCs originate from the transformation of progenitor or mature luminal cells, and the resulting tumors can exhibit histological and/or molecular features of cells undergoing either luminal- or basal-like cell differentiation (4, 5). However, the molecular mechanisms by which luminal tumors acquire basal-like characteristics and generate basal-like BCs (BLBCs) have yet to be elucidated. Importantly, BLBCs constitute the majority (71 to 78%) of human TNBCs (6).

Human BLBCs display many genetic alterations, including *TP53* nonsense and frameshift somatic mutations (84%); aberrant activation of PI3K-AKT pathway genes (*PIK3CA* [49%]; *PTEN* [19%]; *INPP4B* [30%]; *AKT3* [31%]); and activation of RAS-RAF-MEK pathway genes (*KRAS* [32%]; *BRAF* [30%]; *EGFR* [23%]) or other receptor tyrosine kinases (RTKs). Alterations to the *BRCA* (36%), *MYC* (31%), and *RB1* (20%) genes are also observed (6–8). In mice, overexpression of single genes (e.g., *Erbb2*, *Igf-Ir*, *Wnt1*, *Met*, *Notch1-IC* domain, *Stat5*, *H-Ras*, or *Myc*) as well as inactivation of *Trp53*, *Pten*, *Rb*, *Stat1*, *Brg1*, or *Apc* all trigger the development of some form of BC-like malignancies but only after a prolonged period (9). BLBCs do arise after several months in *Brca1+Trp53* (10) and *Rb+Trp53* (11) double heterozygous mutant mice, but, to date, the mouse model showing the quickest onset of BLBC (within 2 wk) features a dominant stable β-catenin mutation combined with exogenous *Met* overexpression (12). Thus, no

Author contributions: H.S., M.N., K.N., T.F., T. Maehama, and A.S. designed research; H.S., M.N., J.O., and T. Maehama performed research; T.S., S. Takao, S.H., T. Masuda, K.M., J.P.L., and H.N. contributed new reagents/analytic tools; J.O., S. Toyokuni, and T. Maehama analyzed data; S. Toyokuni, K.N., and T.F. provided supervision; T. Maehama and A.S. provided project administration; J.P.L. and A.S. provided funding acquisition; and H.S., T. Maehama, and A.S. wrote the paper.

The authors declare no competing interest.

This article is a PNAS Direct Submission.

[1]H.S. and M.N. contributed equally to this work.

[2]T.M. and A.S. contributed equally to this work.

[3]To whom correspondence may be addressed. Email: suzuki@med.kobe-u.ac.jp or tmaehama@med.kobe-u.ac.jp.

This article contains supporting information online at http://www.pnas.org/lookup/suppl/doi:10.1073/pnas.2123134119/-/DCSupplemental.

Published July 11, 2022.

mouse model currently available both exhibits an endogenous single pathway alteration and quickly and faithfully replicates the generation of human BLBC.

Our previous work has revealed the importance of the Hippo–transcriptional coactivator with PDZ-binding motif (TAZ)/yes-associated protein-1 (YAP1) pathway in the development of many types of cancers (13). The Hippo signaling pathway is activated in response to changes in the extracellular environment, including the presence of excessive estrogen (14). The downstream targets of Hippo signaling are the transcriptional cofactors TAZ and YAP1. In most cell types, TAZ and YAP1 positively regulate cell proliferation via their effects on Transcriptional enhanced associated domain (TEAD) transcription factors but are negatively controlled by upstream Hippo pathway elements. These elements include the STE20-like protein kinases, the large tumor suppressor homolog (LATS) kinases, and their adaptor proteins Salvador homolog-1 and Mps one binder kinase activator-1 (MOB1) (14).

Both TAZ and YAP1 are involved in promoting the proliferation, migration, self-renewal, epithelial-mesenchymal transition (EMT), metastasis, and drug resistance of both mouse and human BC cells in vitro (15, 16). However, transgenic (Tg) mice overexpressing either TAZ or YAP1 do not spontaneously develop tumors even in extreme old age (17, 18). TAZ Tg mice did exhibit BC formation after administration of the carcinogen, 7,12-dimethylbenz[a]anthracene (DMBA) (18), although whether these tumors were luminal or basal-like in character was not reported. In humans, while there is some evidence that TAZ is activated in at least the later stages of BC development, especially that of BLBCs, it remains controversial whether the same is true for YAP1 activation (19–22). Moreover, TAZ/YAP1 expression has yet to be examined in human BLBC at its premalignant or carcinoma *in situ* (CIS) stages.

To resolve these issues and elucidate whether Hippo-TAZ/YAP1 activation participates in the onset and progression of BCs, we generated MOB1-deficient mice in which endogenous TAZ and YAP1 were strongly activated in normal mammary luminal cells. We also analyzed TAZ/YAP1 activation in tissue samples from patients with premalignant stage BC. We report that Hippo-TAZ signaling is a key driver of BLBC in mice and that TAZ activation is a feature of early-stage human BLBCs, making the Hippo pathway a worthy therapeutic target.

Results

Loss of *Mob1a/b* Triggers Early Onset of BC in Mice. To examine the roles of TAZ and YAP1 in mature mouse mammary gland, we first sought to generate adult mutant mice that could undergo postnatal deletion of MOB1A and MOB1B, leading to hyperactivation of endogenous TAZ/YAP1 activity. To this end, we crossed *Mob1a*$^{flox/flox}$;*Mob1b*$^{-/-}$ mice (23) to *Rosa26-CreERT2*-Tg mice (24) to produce *Rosa26-CreERT2;Mob1a*$^{flox/flox}$;*Mob1b*$^{-/-}$ progeny in which *Mob1a/b* deletion (double knockout; DKO) could be postnatally induced by treatment with tamoxifen (TAM). We then intraperitoneally (i.p.) administered TAM to *Rosa26-CreERT2;Mob1a*$^{flox/flox}$;*Mob1b*$^{-/-}$ (*ro*Mob1 DKO) mice, as well as to control *Rosa26-CreERT2;Mob1a*$^{+/+}$;*Mob1b*$^{+/+}$ mice, when the animals were 8 to 12 wk old. A test of this strategy using *Rosa26-CreERT2;Mob1a*$^{+/+}$;*Mob1b*$^{+/+}$;*Rosa26-LSL-tdTomato* mice revealed that by 3 wk after TAM initiation (post-TAM), this system had deleted 35, 37, and 3% of luminal, basal, and stromal cells, respectively, from among lineage-negative (CD31^{-}CD45^{-}TER119^{-}) cells isolated from whole mammary glands (*SI Appendix*, Fig. S1*A*). The *Mob1a* gene was deleted frequently (50%) in proximal MECs of *ro*Mob1 DKO mice at 3 wk post-TAM, but only infrequently (10%) in distal MECs (*SI Appendix*, Fig. S1*B*). Loss of MOB1 protein in EpCAM$^{med/high}$ proximal MECs isolated from *ro*Mob1 DKO mice at 3 wk post-TAM was confirmed by immunoblotting (*SI Appendix*, Fig. S1*C*).

We then sacrificed *ro*Mob1 DKO and control mice at 2.5 and 5 wk post-TAM and histologically analyzed their mammary glands. To our surprise, all of the *ro*Mob1 DKO mice had developed tumors in proximal mammary ducts by 2.5 wk post-TAM; (Fig. 1*A*; yellow arrowhead), with 83% of these animals showing ductal CIS (DCIS) and 17% displaying low-grade invasive ductal carcinoma (IDC). Strikingly, all *ro*Mob1 DKO mice exhibited IDC by 5 wk post-TAM. No tumors were observed in TAM-treated control (*Mob1a*$^{flox/flox}$;*Mob1b*$^{-/-}$) mice. In addition, mutant MECs showed hyperplasticity, with many mitotic cells (Fig. 1*B*, green arrowheads) exhibiting impaired cell polarity and containing abnormally large nuclei (Fig. 1*B*, red arrowhead), consistent with malignant transformation. However, all *ro*Mob1 DKO mice died by 10 wk post-TAM (Fig. 1*C*). In previous work, we showed that *ro*Mob1 DKO mice develop tongue cancers (25) and suffer from reduced saliva secretion (26) in response to TAM-induced MOB1 depletion, effects that may have contributed to a fatal impairment of food intake. Our *ro*Mob1 DKO mice were, thus, unsuitable for further BC analyses.

To observe the long-term effects of MOB1 loss in the context of BC development, we generated mammary luminal cell-specific *Mob1a/b* DKO mutants using *Progesterone receptor-Cre knock-in* (*PGR-Cre*) mice (27). We successively mated *PGR-Cre Tg* mice with *Mob1a*$^{flox/flox}$ and *Mob1b*$^{-/-}$ mice to generate *PGR-Cre;Mob1a*$^{flox/flox}$;*Mob1b*$^{-/-}$ mice (*pr*Mob1 DKO mice). This system can delete a target gene starting at E16.5 (28), the time when PGR begins to be expressed in mouse mammary glands, uterus, vagina, and ovaries (27). A test of this strategy using 6-wk-old *PGR-Cre;Mob1a*$^{+/+}$;*Mob1b*$^{+/+}$;*Rosa26-LSL-YFP* mice revealed that, in whole mammary glands, this system had deleted the target gene in 62% of luminal cells but failed completely to delete the target gene in basal cells (*SI Appendix*, Fig. S2 *A* and *B*). The *Mob1a* gene was deleted in 90% of proximal mammary ducts, and in 50% of distal mammary ducts, in *pr*Mob1 DKO mice at 6 wk of age (*SI Appendix*, Fig. S2*C*). *Mob1a*$^{+/+}$;*Mob1b*$^{+/+}$, *Mob1*$^{flox/flox}$;*Mob1b*$^{-/-}$, and *PGR-Cre*;*Mob1a*$^{+/+}$;*Mob1b*$^{+/+}$ mice at 6 wk of age were all indistinguishable from wild-type (WT) mice in gross appearance, survival, and histology (*SI Appendix*, Fig. S2*D*), allowing the use of *Mob1a*$^{flox/flox}$;*Mob1b*$^{-/-}$ mice as the control in subsequent experiments.

Although all *pr*Mob1 DKO mice appeared healthy at birth and most survived for more than 40 wk, 70% of these mutants died by 60 wk of age. In total, 62% of *pr*Mob1 DKO mice developed DCIS in the proximal mammary ducts by 2 wk of age (Fig. 1*D*–*F*), and all developed low-grade IDC by 6 wk of age (Fig. 1*E*). Even from the exterior, proximal DCs of >5 mm in size were obvious from 10 wk of age on (Fig. 1*D*, *Right*). By 40 wk of age, high-grade IDC had developed and metastasized to the lung in 50% of mutant mice, as well as to the lymph nodes (8.3%) and liver (8.3%) (Fig. 1*E* and *G*). These carcinomas appeared in both proximal (yellow arrowhead) and distal (blue arrowhead) ducts (Fig. 1*D*). There were no significant differences in ductal length, or in numbers of terminal endpoints or branch points of the ducts, between control and *pr*Mob1 DKO mice of 6 or 10 wk of age (*SI Appendix*, Fig. S3 *A* and *B*). The most prominent cancerous lesions were observed in the proximal large ducts of *pr*Mob1 DKO mice (Fig. 1*D*–*F*). Detailed pathological analysis confirmed the successive occurrence of usual ductal hyperplasia

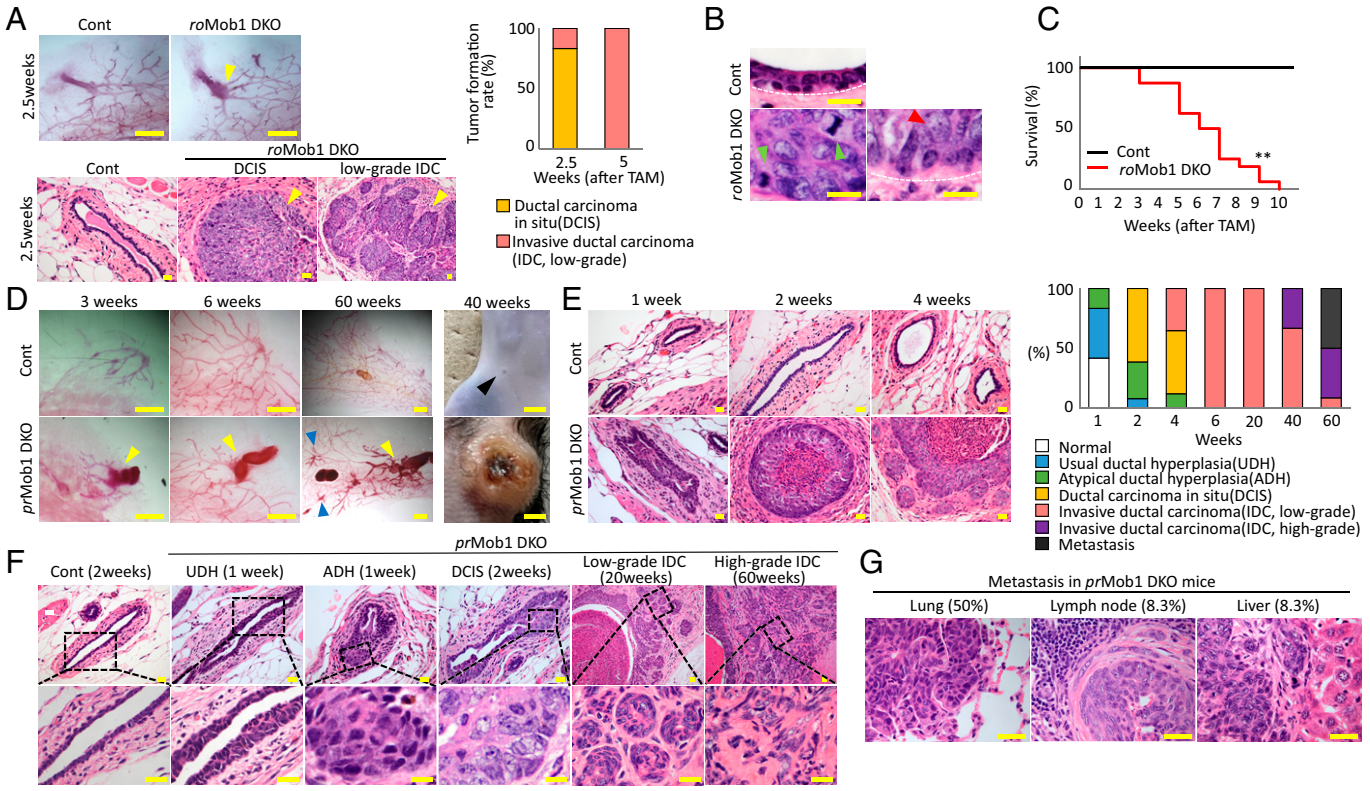

Fig. 1. *Mob1a/b* deletion in adult mouse mammary epithelium results in extremely rapid carcinogenesis. (*A*) (*Left*) Representative carmine-stained stereomicroscopic views (*Top*) and hematoxylin and eosin (H&E)-stained microscopic views of sections (*Bottom*) of control and *ro*Mob1 DKO mammary epithelial layers at 2.5 wk post-TAM administration. Yellow arrowheads, tumors in proximal large ducts. Scale bars, 2 mm (*Top*) and 20 μm (*Bottom*). (*Right*) Percentages of the indicated lesion types in mammary epithelium of *ro*Mob1 DKO mice at the indicated weeks post-TAM (n = 10/group). (*B*) H&E-stained sections of control (*Top*) and *ro*Mob1 DKO (*Bottom*) mammary epithelial layers at 2.5 wk post-TAM. Mutant epithelium shows features of CIS, including hyperplasia with many mitotic cells (green arrowheads) exhibiting impaired cell polarity and abnormally large nuclei (red arrowhead). White dotted line, basement membrane. Scale bars, 20 μm. (*C*) Kaplan-Meier curves depicting overall survival of TAM-treated *ro*Mob1 DKO and control mice (n = 16). $^{**}P < 0.01$, Log-rank test. (*D*) (*Left*) Representative carmine-stained stereomicroscopic views of mammary glands of control and *pr*Mob1 DKO mutant mice at the indicated weeks of age. Yellow or blue arrowheads indicate tumors in proximal or distal mammary ducts, respectively. (*Top Right*) Macroscopic view of control mammary gland at 40 wk. Black arrowhead, nipple. (*Bottom Right*) Macroscopic view of tumor formation in *pr*Mob1 DKO mammary gland at 40 wk. Scale bars, 2 mm. (*E*) (*Left*) Representative H&E-stained mammary tissues from control and *pr*Mob1 DKO mice (n = 12 to 17 mice/group/timepoint) sacrificed at the indicated weeks after birth. Actively growing CIS was observed in *pr*Mob1 DKO mice from 2 wk of age onward. Scale bars, 20 μm. (*Right*) Percentages of *pr*Mob1 DKO mice showing the indicated grades of mammary tumors at the indicated weeks after birth. (*F*) Low magnification (*Top*) and high magnification (*Bottom*) views of representative H&E-stained mammary duct epithelial layers from control and *pr*Mob1 DKO mice at the indicated weeks of age. As they aged, mutant mice successively developed UDH, ADH, DCIS, low-grade IDC, and high-grade IDC. Scale bars, 20 μm. (*G*) Representative H&E-stained sections of lung, lymph node, and liver tissues that were isolated from 60-wk-old *pr*Mob1 DKO mice and exhibited metastasis of malignant MECs. Scale bars, 20 μm.

(UDH), atypical ductal hyperplasia (ADH), DCIS, low-grade IDC, and finally high-grade IDC in *pr*Mob1 DKO mice as they aged (Fig. 1*F*). Unfortunately, due to the female infertility of both *pr*Mob1 DKO and *ro*Mob1 DKO mice, we were unable to examine mammary gland alterations during pregnancy and lactation. Nevertheless, both TAM-treated *ro*Mob1 DKO mice and *pr*Mob1 DKO mice showed surprisingly rapid onset and development of BCs, and so provided suitable models for further mechanistic analyses.

Luminal-Cell-Specific MOB1-Deficient Mice Develop TN BLBCs. To classify the BCs in our *pr*Mob1 DKO mice, we performed immunohistochemistry (IHC) studies of tumor sections that were isolated from *pr*Mob1 DKO mice at 10 wk of age and stained using antibodies against KRT8, ESR, KRT14, KRT5, or p63. KRT8 and ESR are luminal cell markers, whereas KRT14, KRT5, and p63 are basal cell markers. We found that all BCs in *pr*Mob1 DKO mice were ESR^{-}, $KRT8^{-}$, $KRT14^{+}$, $KRT5^{+}$, and $p63^{+}$, classifying them as BLBC (Fig. 2*A*). We confirmed this finding using qPCR and flow cytometric analysis of $EpCAM^{med/high}$ proximal MECs isolated from control and *pr*Mob1 DKO mice at 10 wk of age. qPCR revealed that messenger RNA (mRNA) levels of the basal cell markers *Krt14*, *Krt5*, and *Tp63* were increased (Fig. 2*B*, *Left*), while those of the luminal cell markers *Krt8*, *Esr1*, *Pgr*, *Foxa1*, and *Her2/Erbb2* were all decreased (Fig. 2*B*, *Middle*). Increased mRNA levels of *Ctgf* and *Ankrd1*, which are downstream targets of TAZ/YAP1, were also observed and constituted a positive control (Fig. 2*B*, *Right*). Similarly, flow cytometric analysis showed that the basal cell population ($CD24^{med}CD49f^{high}$) was increased in *pr*Mob1 DKO mice, whereas the luminal cell population ($CD24^{high}CD49f^{med}$) was decreased (Fig. 2*C*).

Because BLBC originates from luminal cells (4), we used IHC to monitor changes to luminal and basal cell markers in tumors developing in *pr*Mob1 DKO mice as they aged. At 2 wk of age, *pr*Mob1 DKO mice showed increased numbers of $KRT8^{+}$ luminal tumor cells in the proximal ducts, with approximately normal numbers of $KRT5^{+}$ basal cells (Fig. 2*D*, *Left*). However, the level of KRT8 expression by tumor cells then gradually declined, and the number of $KRT5^{+}$ tumor cells increased. Importantly, by 6 wk of age, as many as 37% of tumor cells were $KRT8^{+}KRT5^{+}$ in phenotype (Fig. 2*D*, *Right*). By 10 wk of age, almost all $KRT8^{+}$ tumor cells had

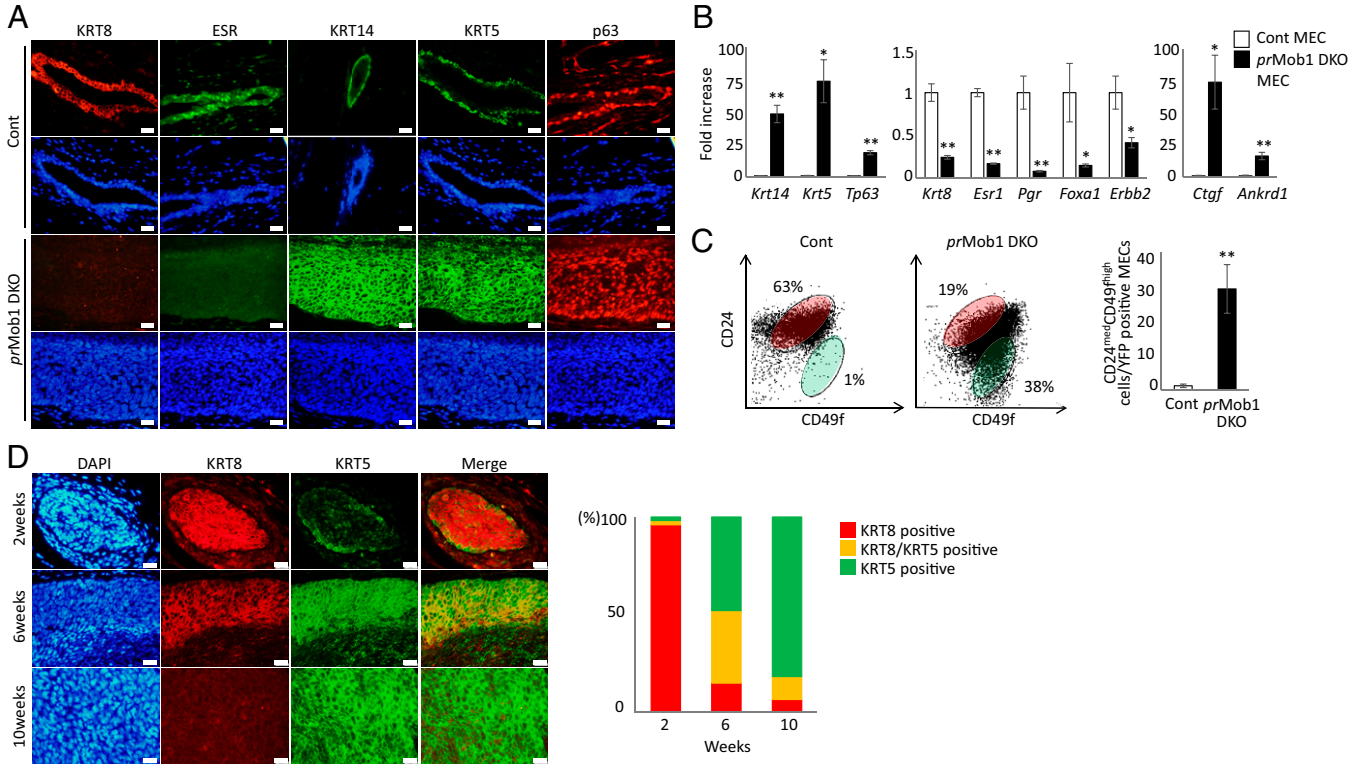

Fig. 2. Tumors in luminal-cell-specific MOB1-deficient mice are TN basal-like in phenotype. (*A*) Representative immunostaining to detect KRT8, ESR, KRT14, KRT5, or p63, as indicated, in sections of (*Top*) normal mammary epithelium from a control mouse or (*Bottom*) BCs resected from *pr*Mob1 DKO mice at 10 wk of age. Scale bars, 20 μm. (*B*) (*Left* and *Middle*) Quantitation of the fold increase or decrease in mRNA expression of the basal (*Krt14*, *Krt5*, *Tp63*) and luminal (*Krt8*, *Esr1*, *Pgr*, *Foxa1*, *Erbb2*) markers as determined by qPCR in EpCAM$^{med/high}$ proximal MECs isolated from control and *pr*Mob1 DKO mice at 10 wk of age. mRNA expression data were normalized to *Gapdh*. Data are the mean ± SEM (n = 4/group). (*Right*) mRNA levels of the Hippo-TAZ/YAP1 downstream target genes *Ctgf* and *Ankrd1*, which were analyzed as positive controls. *P < 0.05 and **P < 0.01, t test. (*C*) (*Left*) Representative flow cytometric analysis to detect CD24^{high}CD49f^{med} luminal cells and CD24^{med}CD49f^{high} basal cells among EpCAM$^{med/high}$ proximal MECs isolated from control or *pr*Mob1 DKO mice at 10 wk of age. (*Right*) Quantification of the ratio of CD24^{med}CD49f^{high} basal cells to total YFP^{+} MECs for the cells in the left panels. Data are the mean ± SEM (n = 3 mice/group). **P < 0.01, t test. (*D*) (*Left*) Representative immunostaining to detect KRT8 (red) and KRT5 (green) in tumors isolated from *pr*Mob1 DKO mice at 2, 6, and 10 wk of age. 4′,6-diamidino-2-phenylindole (DAPI) (blue), nuclei. Scale bars, 20 μm. (*Right*) Percentages of KRT5^{+}, KRT8^{+}/KRT5^{+}, and KRT8^{+} cells among mammary tumor cells isolated from *pr*Mob1 DKO mice at the indicated ages.

disappeared, leaving a few remaining KRT8^{+}KRT5^{+} cells among a vast pool of KRT5^{+} BLBC cells. Thus, in the absence of MOB1, luminal cells become transformed over time, gradually losing their luminal character and gaining basal-like features until they generate a TN (ESR^{-}PGR^{-}HER2^{-}) BLBC.

Onset of BC in MOB1-Deficient Mice Depends on TAZ Activation. IHC analysis demonstrated that, in control mice, TAZ was activated mainly in luminal cells of large ducts but only faintly expressed in luminal cells of small ducts, both at the prepuberty and puberty virgin stages (Fig. 3*A* and *B*). TAZ expression was even weaker in the basal cells of the large ducts in control mice (Fig. 3*A* and *C*). Pregnancy and lactation increased TAZ expression in the large ducts (Fig. 3*A* and *C*). On the other hand, MOB1 was expressed in both luminal and basal cells, in both large and small ducts, and during both the prepuberty and puberty virgin periods in control mice. Furthermore, MOB1 expression was markedly reduced in pregnant control mice, with only a modest increase during the lactation period (*SI Appendix*, Fig. S4*A* and *B*). These results are in line with MOB1's expected negatively regulatory effect on TAZ activation in the mammary ducts of control mice, especially in the large ducts. TAZ was expressed more strongly in the luminal cells of large ducts and tumors of *pr*Mob1 DKO and *ro*Mob1 DKO mice compared to controls (Fig. 3*A* and *D*). TAZ nuclear staining intensity in the small ducts of *pr*Mob1 DKO and *ro*Mob1 DKO mice was weaker than that in the large ducts but still stronger than that in controls (Fig. 3*A* and *E*). Because both *pr*Mob1 DKO and *ro*Mob1 DKO female mice are infertile, we could not examine TAZ activation during pregnancy or lactation in these animals.

With respect to YAP1, the immunostaining revealed faint activation of YAP1 in the basal cells of control large ducts, but the activation was negligible in *ro*Mob1 DKO mammary tumors at 5 wk post-TAM. However, YAP1 was strongly activated in the nuclei of epidermal skin cells of the same mutant mice (Fig. 3 *F* and *G*). These observations suggest that the function of TAZ, but not YAP1, was affected by mammary-tissue-specific loss of MOB1.

To investigate the roles of TAZ and YAP1 in the phenotypes of MOB1-deficient MECs, we crossed *ro*Mob1 DKO, *Yap1*$^{flox/flox}$, and *Taz*$^{flox/flox}$ mice to generate triple KO (TKO) mutants either lacking TAZ plus MOB1 (*Rosa26-CreERT2;Mob1a*$^{flox/flox}$*; Mob1b*$^{-/-}$*;Taz*$^{flox/flox}$; designated *ro*Mob1TAZ TKO) or lacking YAP1 plus MOB1 (*Rosa26-CreERT2;Mob1a*$^{flox/flox}$*;Mob1b*$^{-/-}$*; Yap1*$^{flox/flox}$; designated *ro*Mob1YAP1 TKO). The onset of tumors in MOB1-deficient mammary epithelium was completely prevented by additional deficiency of TAZ, but not by deficiency of YAP1 (Fig. 3*H* and *I*). This result confirms our hypothesis that the onset of mammary tumorigenesis associated with MOB1 deficiency depends largely on TAZ, but not on YAP1, and aligns with our observation that BC arises in luminal cells of MOB1-deficient large ducts, where TAZ activation is the strongest.

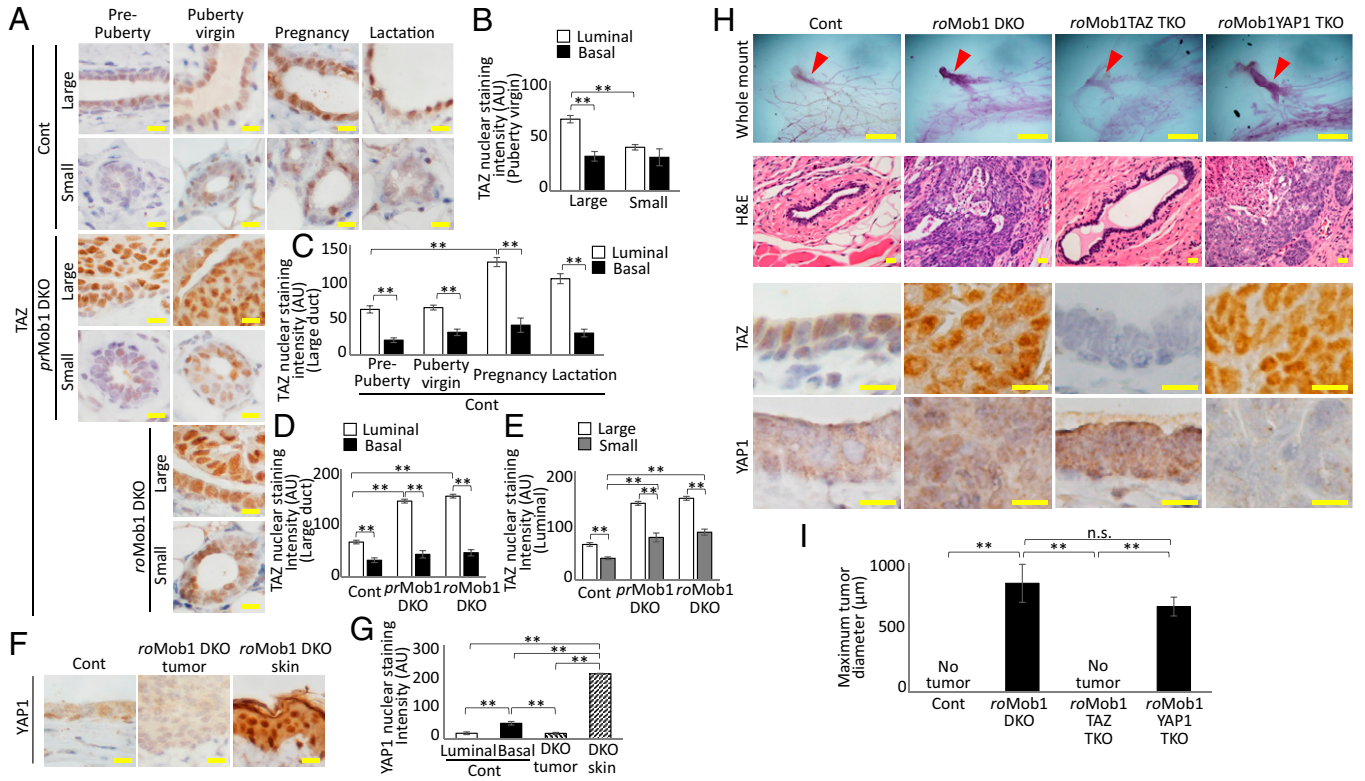

Fig. 3. MOB1-mediated TAZ activation controls the onset of mammary tumors in mice. (*A*) Representative immunostaining to detect TAZ protein in control, *pr*Mob1 DKO, and *ro*Mob1 DKO mammary epithelium at the prepuberty (1 to 3 wk), puberty virgin (8 to 12 wk), pregnancy, and lactation stages. Large and small ducts were distinguished by their localization and size as described in *SI Appendix, Supplementary Methods* and were analyzed separately. Scale bars, 10 μm. (*B*) Quantitation of the intensity of TAZ nuclear staining in luminal and basal cells in the large and small ducts of control mice at the puberty virgin stage ($n = 4$). (*C*) Quantitation of TAZ nuclear staining intensity of luminal and basal cells in the large ducts of control mice at the indicated stages (prepuberty, $n = 4$; puberty virgin, $n = 4$; pregnancy, $n = 4$; lactation, $n = 4$). (*D*) Quantitation of TAZ nuclear staining intensity of luminal and basal cells in the large ducts of control ($n = 4$), *pr*Mob1 DKO ($n = 4$), and *ro*Mob1 DKO ($n = 4$) mice at the puberty virgin stage. (*E*) Quantitation of TAZ nuclear staining intensity of luminal cells in the large and small ducts of control ($n = 4$), *pr*Mob1 DKO ($n = 4$), and *ro*Mob1 DKO ($n = 4$) mice at the puberty virgin stage. (*F*) Representative immunostaining to detect YAP1 protein in (*Left*) control large duct, (*Middle*) *ro*Mob1 DKO mammary tumor, and (*Right*) *ro*Mob1 DKO epidermis at 5 wk post-TAM. Scale bars, 10 μm. (*G*) Quantitation of YAP1 nuclear staining intensity in luminal (white bar) and basal (black bar) cells in the control large duct, *ro*Mob1 DKO mammary tumor, and *ro*Mob1 DKO epidermis (hatched bars) samples in *F*. For *B*–*E* and *G*, at least 20 cells were analyzed for each sample, and staining intensity was measured by ImageJ in AUs. Data are the mean ± SEM $^{**}P < 0.01$, Tukey's multiple comparison test. (*H*) (*Top*) Representative carmine-stained stereomicroscopic views of whole mounts of mammary glands from mice of the indicated genotypes at 5 wk post-TAM. Scale bars, 2 mm. (*Middle*) H&E-stained sections of proximal large ducts in mammary epithelium of the mice in the top row. Scale bars, 20 μm. (*Bottom*) Immunostaining to detect TAZ and YAP1 in proximal large ducts in mammary epithelium of the mice in the top row. Scale bars, 10 μm. (*I*) Quantitation of the maximum diameter of tumors estimated from serial sections of proximal ducts in mice of the indicated genotypes at 5 wk post-TAM. Data are the mean ± SEM ($n = 6$ mice/group). $^{**}P < 0.01$, n.s., not significant, *t* test.

Alterations to Hippo-TAZ Signaling Result in a Gain of Tumorigenic Properties and a Shift toward BLBC. We next established mammary organoid cultures using luminal cells that were purified from *ro*Mob1 DKO or control mice and cultured with or without TAM for 14 d *in vitro*. Both the number and size of organoids derived from *ro*Mob1 DKO luminal cells were significantly increased by TAM treatment (Fig. 4*A* and *B*). Enhanced cell proliferation in MOB1-deficient organoids was confirmed by their significantly increased $Ki67^+$ positivity (Fig. 4*C* and *D*). Notably, terminal deoxynucleotidyl transferase-mediated dUTP nick end labeling $(TUNEL)^+$ apoptotic cells were very rare in both control and MOB1-deficient luminal cell cultures (*SI Appendix*, Fig. S5*A* and *B*). Thus, MOB1 deficiency confers increases in progenitor-like activities and proliferation on luminal cells.

To support our mammary organoid observations, we examined the TAZ-dependent tumorigenic properties of the human MEC line MCF10A-*i*TAZ4SA, which inducibly expresses a constitutively active mutant form of TAZ (TAZ4SA) (29) in response to doxycycline (Dox) treatment (*SI Appendix*, Fig. S6*A*). As expected, forced TAZ activation in MCF10A cells increased their proliferation (*SI Appendix*, Fig. S6*B*). The incidence of multipolar mitotic spindle formation in these cells (Fig. 4*E* and *F*) and the emergence of micronuclei (Fig. 4*G* and *H*) were also enhanced. The number of apoptotic MCF10A cells was also modestly elevated by constitutive TAZ activation (*SI Appendix*, Fig. S6*C*). These results suggest that TAZ-induced increases in cell proliferation, progenitor-like activities, and chromosomal mis-segregation may drive tumor onset in MOB1-deficient mammary glands.

Because the MOB1-deficient luminal cancers in our mutant mice had acquired a basal-like phenotype upon TAZ activation *in vivo*, we examined whether TAZ activation in a human luminal cancer cell line (MCF7) would induce these cells to adopt a basal-like cancer phenotype *in vitro*. For this purpose, we engineered MCF7 cells to overexpress *i*TAZ4SA (MCF7-*i*TAZ4SA cells). We then cultured these cells with or without Dox for 7 d and analyzed the expression of luminal and basal markers by qPCR (Fig. 4*I*) and immunofluorescence staining (Fig. 4*J*). Overexpression of activated TAZ4SA complementary DNA resulted in strong expression of TAZ at both the mRNA and nuclear protein levels and also upregulated the mRNA expression of TAZ downstream transcriptional targets. As expected, the expression of constitutively active TAZ induced by Dox treatment also increased mRNA levels of *KRT14*, *KRT5*, *EGFR*, and *KRT17* (basal markers) while decreasing those of *KRT8*, *ESR*,

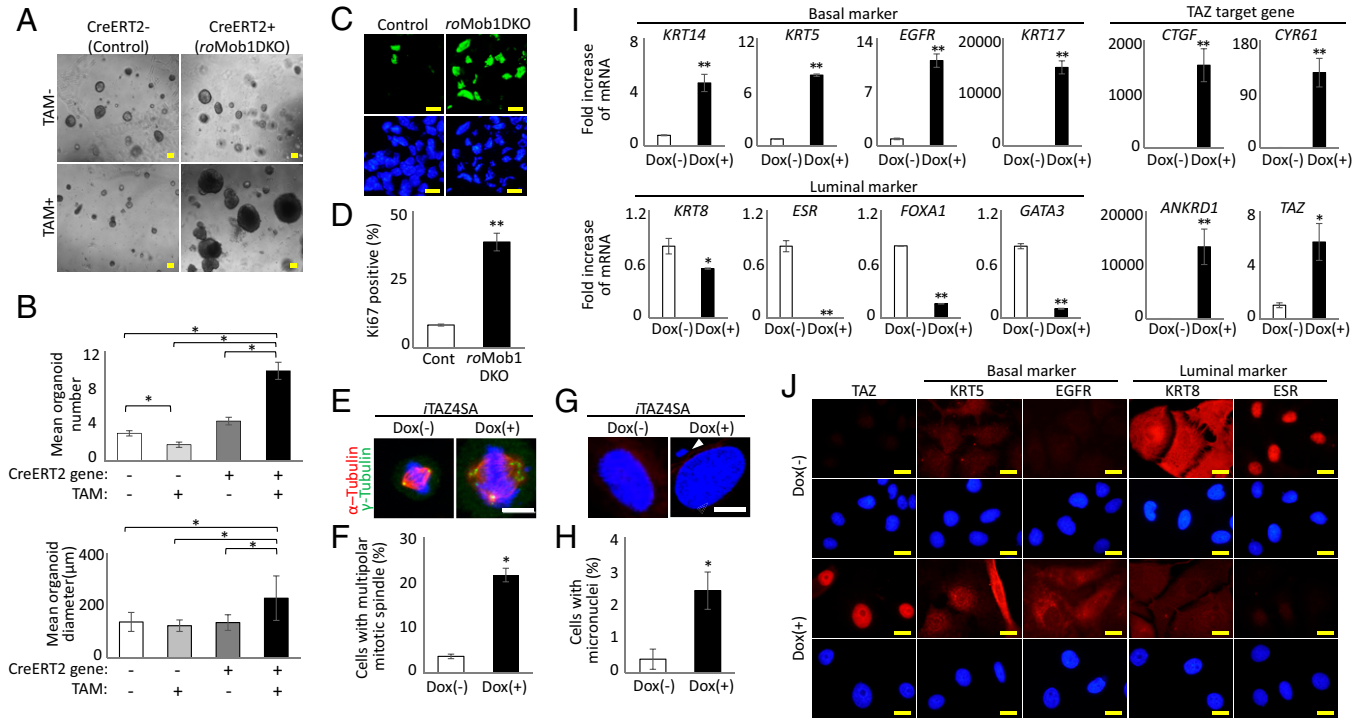

Fig. 4. Tumorigenic properties of mammary cells bearing MOB1-TAZ alterations and effect of TAZ overexpression on luminal BC cells in vitro. (*A*) Macroscopic views of representative organoids generated by culturing luminal cells that were purified from *ro*Mob1 DKO and control mice. Cells were treated with or without TAM for 2 d, followed by the incubation in Matrigel without TAM for 12 d in vitro. Scale bars, 100 μm. (*B*) Quantitation of the (*Top*) mean number and (*Bottom*) mean diameter of the organoids in *A*. Data shown are the mean ± SEM (n = 3/group). *P < 0.05, Tukey's multiple comparison test. (*C*) Representative images of Ki67 staining of the organoids in *A*. Nuclei were counterstained with DAPI. Scale bars, 20 μm. (*D*) Quantitation of the Ki67-positive cells in *C*. At least 1,000 cells were counted for each sample. Data are the mean ± SEM (n = 3). **P < 0.01, t test. (*E*) Immunostaining to detect α-tubulin (red) and γ-tubulin (green) in MCF10A-*i*TAZ4SA cells that were cultured with or without Dox for 7 d. DAPI (blue), nuclei. (*Left*) Representative normal mitotic cell (Dox−). (*Right*) A mitotic cell overexpressing TAZ4SA (Dox+) showing a multipolar spindle. Scale bar, 10 μm. (*F*) Quantitation of cells with multipolar mitotic spindles in the Dox+ and Dox− MCF10A-*i*TAZ4SA cultures in *E*. At least 50 mitotic cells/sample were evaluated. Data are the mean ± SEM (n = 3). *P < 0.05, t test. (*G*) Immunostaining to detect α-tubulin (red) and nuclei (DAPI, blue) in MCF10A-*i*TAZ4SA cells that were cultured with or without Dox for 7 d. (*Left*) Representative normal cell showing a normal nucleus (Dox−). (*Right*) A cell overexpressing TAZ4SA (Dox+) showing a micronucleus (white arrowhead). Scale bar, 10 μm. (*H*) Quantitation of cells with micronuclei in the Dox− (n = 3) and Dox+ (n = 5) MCF10A-*i*TAZ4SA cultures in *G*. At least 130 cells/sample were evaluated. Data are the mean ± SEM. *P < 0.05, t test. (*I*) Quantitation of mRNA levels of (*Top Left*) the basal cell marker genes *KRT14*, *KRT5*, *EGFR*, and *KRT17;* (*Bottom Left*) the luminal cell marker genes *KRT8*, *ESR*, *FOXA1*, and *GATA3;* and (*Right*) TAZ and its target genes *CTGF*, *CYR61*, and *ANKRD1* in MCF7-*i*TAZ4SA cells that were cultured for 7 d with or without Dox (1 μg/mL). Data are the mean ± SEM (n = 3). *P < 0.05 and **P < 0.01, t test. (*J*) Representative immunofluorescent staining of TAZ, basal cell marker (KRT5, EGFR), and luminal cell marker (KRT8, ESR) proteins in MCF7-*i*TAZ4SA cells that were cultured for 7 d with or without Dox (1 μg/mL). DAPI (blue), nuclei. Scale bars, 20 μm.

FOXA1, and *GATA3* (luminal markers) (Fig. 4*I*). Consistent with these results, the basal proteins KRT5 and EGFR were increased in MCF7-*i*TAZ4SA cells, but the luminal proteins KRT8 and ESR were decreased (Fig. 4*J*). Thus, constitutive and aberrant activation of TAZ can convert human luminal BC cells into BLBC cells in vitro.

TAZ Activation in Human Premalignant BLBC. To our knowledge, the status of TAZ activation has not been examined in human premalignant mammary tissues, including in DCIS. We therefore sought to examine TAZ immunostaining intensity in normal human breast tissue samples as well as in patient tissue samples exhibiting UDH, ADH, DCIS, or IDC lesions. First, we evaluated the specificity of an antibody against human TAZ by immunostaining of WT, YAP1-KO, and TAZ-KO variants of the human non-small-cell lung cancer cell line H1299-Luc. This anti-TAZ antibody did not stain TAZ-KO H1299-Luc cells but generated a clear positive signal for both parental H1299-Luc and YAP1-KO H1299-Luc cells (*SI Appendix*, Fig. S7*A*). Deficiency of YAP1 and TAZ proteins in YAP1-KO and TAZ-KO variants, respectively, were confirmed by immunoblotting (*SI Appendix*, Fig. S7*B*). Thus, we deemed our anti-human TAZ antibody to be suitable for the specific detection of TAZ in human BC specimens.

Patients with basal-like type DCIS or IDC were selected on the basis of the KRT5 positivity (>50%) of their tumor cells (*SI Appendix*, Fig. S8*A*, *Left*). Immunostaining using anti-TAZ antibody showed that TAZ activation was upregulated from normal levels starting at the premalignant UDH stage, with a gradual increase in TAZ protein detected in both the nucleus and cytoplasm of human MECs as malignancy progressed (Fig. 5*A* and *B*). In contrast, immunostaining to detect YAP1 protein showed a limited and very gradual increase only in the cytoplasm of KRT5$^+$ MECs, with no significant increase in the nucleus even at the DCIS and IDC stages of BLBC (*SI Appendix*, Fig. S8*B*). When we examined ESR$^+$ human luminal BCs in the same way (*SI Appendix*, Fig. S8*A*, *Right*), neither nuclear TAZ (Fig. 5*C* and *D*) nor nuclear YAP1 (*SI Appendix*, Fig. S8*C* and *D*) was increased in DCIS or even IDC samples. To test whether TAZ expression changed during the course of tumor progression in a single patient, we examined five clinical BLBC samples that each contained cancerous lesions of different pathological stages as well as a noncancerous normal tissue area in a single slice of the specimen. Analysis of TAZ nuclear staining intensities in these samples showed that TAZ activation gradually increased with histological progression to BLBC, even within a single specimen (*SI Appendix*,

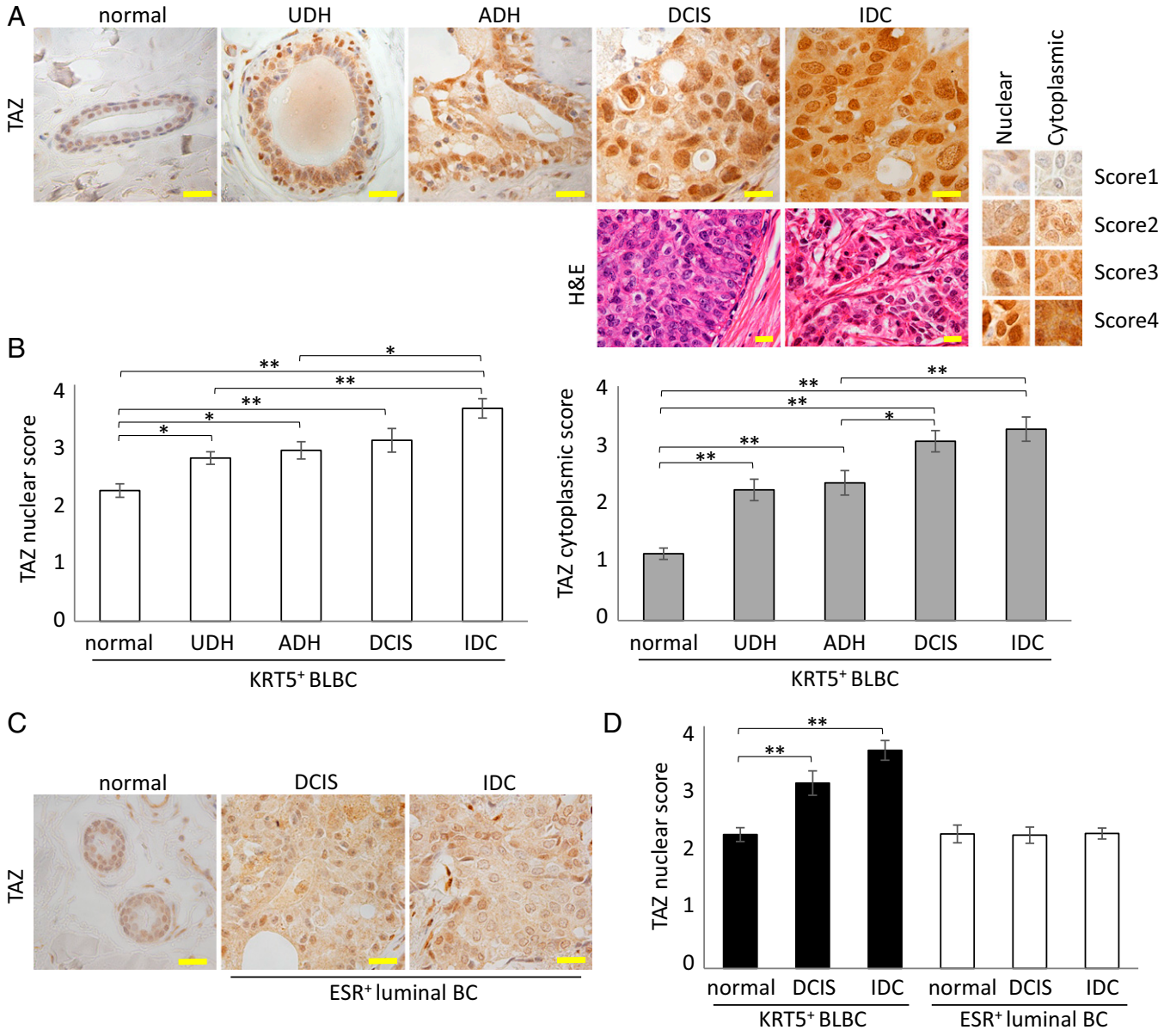

Fig. 5. TAZ activation initiates at the precancerous stage of human BLBC. (*A*) (*Top*) Representative immunostaining to detect TAZ (with hematoxylin counterstaining) in normal proximal mammary duct (n = 14) or in lesions from KRT5$^+$ BLBC patients displaying UDH (n = 17), ADH (n = 17), DCIS (n = 17), or IDC (n = 15). The scoring system to indicate degrees of nuclear and cytoplasmic TAZ staining is also shown. (*Bottom*) H&E-stained sections of DCIS and IDC patient samples. Scale bars, 20 μm. (*B*) Quantitation of the mean nuclear (*Left*) and cytoplasmic (*Right*) TAZ staining scores for normal proximal mammary duct or the indicated lesions from the KRT5$^+$ BLBC patients in *A*. Data are the mean ± SEM (n = 15 or 17/group). *P < 0.05 and **P < 0.01, Tukey's multiple comparison test. (*C*) Representative immunostaining to detect TAZ (with hematoxylin counterstaining) in sections of normal human mammary duct as well as DCIS and IDC lesions from patients with ESR$^+$ luminal BCs. Scale bars, 20 μm. (*D*) Quantitation of mean nuclear TAZ score for normal human proximal mammary ducts (n = 10), and for DCIS (n = 10) and IDC (n = 22) lesions, from patients with KRT5$^+$ BLBC or ESR$^+$ luminal BC, as indicated. Data are the mean ± SEM **P < 0.01, Tukey's multiple comparison test.

Fig. S9*A* and *B*). Thus, the nuclear localization and activation of TAZ in premalignant mammary gland lesions is an event that leads to BLBC.

TP53 Inactivation Following Hippo-TAZ Pathway Alteration Accelerates Tumor Progression. Because the most frequently mutated gene in human invasive BLBCs is *TP53*, we next used IHC to examine *TP53* mutation status in the DCIS stage of human KRT5$^+$ BLBC (Fig. 6*A*). Previous IHC work has linked strong nuclear accumulation of TP53 protein with *TP53* missense mutations, and complete loss of TP53 protein with null *TP53* mutations (30). We found *TP53* mutations in 80% of IDC BLBC patients, consistent with a previous report (31), but in only 5.9% of DCIS BLBC patients (Fig. 6*B*, *Left*). Intriguingly, *TP53* mutation was observed in 0 and 22.7% of DCIS and IDC ESR$^+$ luminal BCs, respectively (Fig. 6*B*, *Right*). Thus, although *TP53* mutation is frequent in BLBC IDC samples, it may not be the primary event driving the onset of BLBC.

To determine the additional effects of TP53 inactivation on neoplasms featuring Hippo-TAZ alterations, we generated *PGR-Cre;Mob1a*$^{flox/flox}$*;Mob1b*$^{-/-}$*;Trp53*$^{flox/flox}$ (*pr*Mob1Tp53 TKO) mice and compared mammary tumor progression in these animals with that in *pr*Mob1 DKO mice. Upon sacrifice at 10 wk of age, *pr*Mob1Tp53 TKO mice showed tumors that were larger in size than those in *pr*Mob1 DKO mice (Fig. 6*C*, *Top* and *D*, *Left*). In *pr*Mob1 DKO mice, tumors were observed only in the proximal mammary ducts, but tumors in *pr*Mob1Tp53 TKO mice infiltrated along these ducts and so

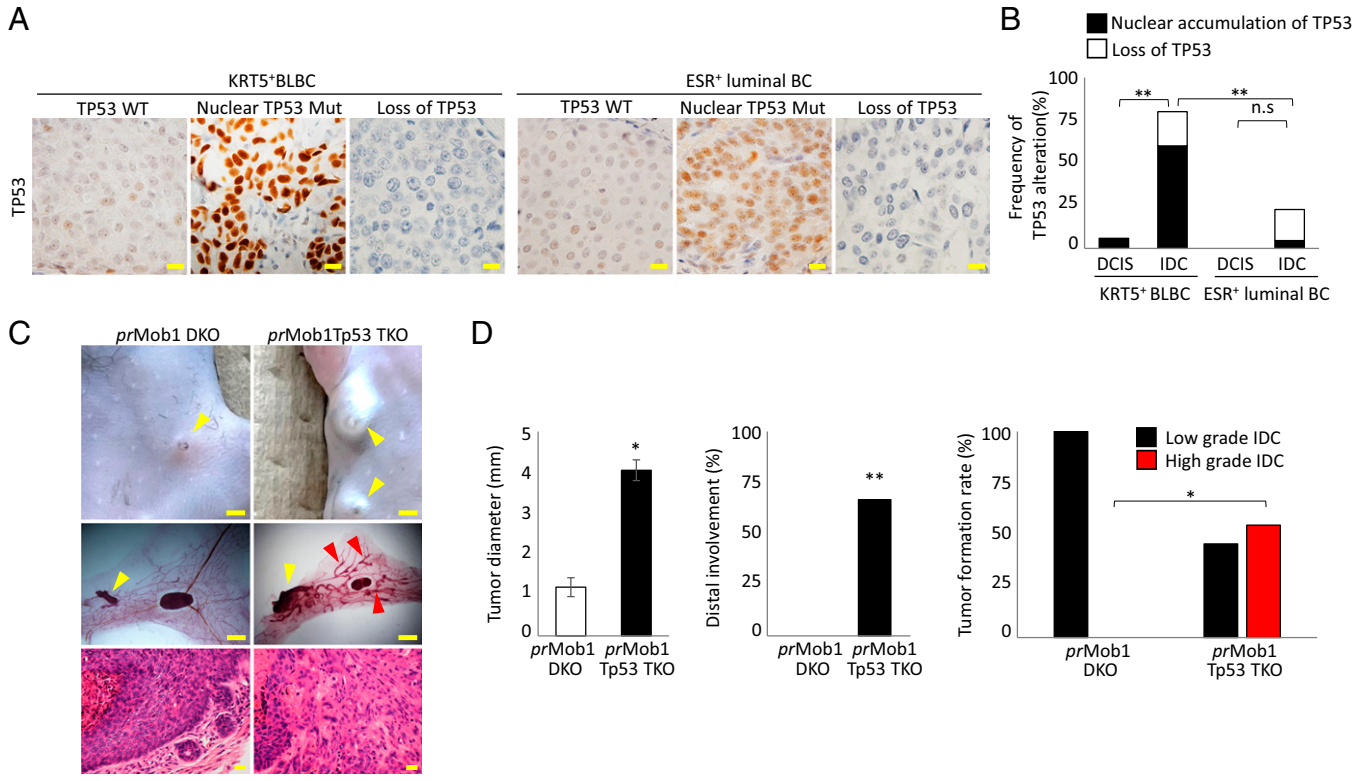

Fig. 6. Frequency of TP53 mutation in DCIS BLBC patients and effect of combined alterations of the Hippo-TAZ pathway plus TP53 in mice. (*A*) Representative immunostaining to detect TP53 (with hematoxylin counterstaining) in sections of human DCIS and IDC from (*Left*) KRT5$^+$ BLBC and (*Right*) ESR$^+$ luminal BC patients. Scale bars, 20 μm. (*B*) Quantitation of TP53 alteration frequency in human DCIS (n = 17) and IDC (n = 15) lesions from the BLBC patients in *A* and in DCIS (n = 10) and IDC (n = 22) lesions from the ESR$^+$ luminal BC patients in *A*. The percentages of tumors showing nuclear accumulation of TP53 (black bars) and TP53-null tumors (white bars) are indicated. Data are the mean ± SEM. $^{**}P < 0.01$, Fisher's exact test. (*C*) Representative macroscopic views (*Top*), carmine-stained stereomicroscopic views (*Middle*), and H&E-stained microscopic views (*Bottom*) of mammary ducts in 10-wk-old *pr*Mob1 DKO and *pr*Mob1Tp53 TKO mice. Yellow arrowheads, tumors in proximal ducts. Red arrowheads, tumors in distal ducts. Scale bars are 2 mm, 2 mm, and 20 μm in macroscopic, stereoscopic, and microscopic views, respectively. (*D*) Quantitation of tumor diameter, percentage of distal involvement, and percentage of high- and low-grade IDC in the *pr*Mob1 DKO and *pr*Mob1Tp53 TKO mice in *C*. Data are the mean ± SEM (n = 10 to 11). $^*P < 0.05$, $^{**}P < 0.01$, t test (*Left*) or Fisher's exact test (*Middle* and *Right*).

also appeared in the distal mammary ducts (Fig. 6*C*, *Middle*, red arrowhead; Fig. 6*D*, *Middle*). Histologically, all tumors in *pr*Mob1 DKO mice were classified as low-grade IDC, but 54.5% of tumors in *pr*Mob1Tp53 TKO mice were considered to be high-grade IDC (Fig. 6*C*, *Lower* and 6*D*, *Right*). Thus, TP53 inactivation subsequent to Hippo-TAZ activation accelerates mammary tumor progression.

Discussion

This study has generated an animal model in which the mutation of a signal element in the Hippo pathway leads to very rapid and spontaneous BC onset. Indeed, our mutant mice show the quickest BC onset and progression induced by any single pathway alteration. Stunningly, all tumors observed in these mutant mice are BLBCs. Because the onset of these malignancies was so fast, we conclude that the Hippo-TAZ pathway is also highly likely to be a key driver of human BLBC. As was true in our mutant mice, it may be that significant activation of Hippo-TAZ signaling can initiate human BLBC in the absence of any other genetic or epigenetic alteration.

This pinpointing of altered Hippo-TAZ signaling as a key factor in human BLBC aligns with known risk factors. Obesity, high estrogen levels, and exposure to tobacco smoke have all been documented to increase BC risk; and lipid accumulation, estrogen treatment, and cigarette smoke extract have all been shown to activate TAZ/YAP1 (32–34). In addition, most of the genetic changes observed in human BLBCs—such as *TP53* mutation or the aberrant activation of the WNT1, PI3K, HIF1α/ARNT, EGFR, or other RTK pathways—can activate TAZ/YAP1 (25, 35–38). These data support our conclusion that events resulting in accumulated TAZ activation might lead to the onset and progression of human BLBC.

Although our MOB1-deficient mice showed rapid BC formation, neither TAZ Tg mice (18) nor YAP1 Tg mice (17) spontaneously develop tumors at any time during their lives. A potential explanation for this discrepancy is that these TAZ Tg and YAP1 Tg animals were generated using the mouse mammary tumor virus (MMTV)-promotor system, which drives gene expression not only in MECs, but also in other tissues such as the salivary glands. It is possible that a Tg mouse strain showing strong TAZ/YAP1 activation in multiple tissues might therefore die prematurely, and that a strain with weak TAZ/YAP1 activation might survive this alteration tumor free. In fact, we have found that most of the MOB1-deficient mice we have generated using the *MMTV-Cre* Tg approach show early lethality due, at least in part, to decreased saliva secretion (*SI Appendix*, Fig. S10). Another possible reason for the lack of tumor formation in TAZ Tg and YAP1 Tg mice is the effect of TAZ/YAP1-independent LATS kinase activity. LATS can bind to and control several molecules besides TAZ/YAP1, including the TP53 E3 ligase MDM2 (39), the ESR (40), the cytokinesis regulator Aurora B (41), and the cell-cycle regulator CDC26 (42). Alteration of these TAZ/YAP1-independent downstream effectors of LATS kinases may be required for BC onset. In fact, significant downregulation of *LATS* mRNA expression in human breast tumors compared to

matched normal tissue has been reported (43). Nevertheless, for mechanistic reasons that remain under investigation, TAZ must be important for BC development because the formation of these malignancies in our MOB1-deficient mice was substantially prevented by additional loss of TAZ.

Previous reports have demonstrated that TAZ overexpression is more often observed in patients with invasive BLBCs (70.8% positive) than in those with invasive ESR^+/PGR^+ (12 to 30% positive) or $HER2^+$ (16 to 19.4% positive) luminal cancers (21, 22), indicating that TAZ activation is especially important in invasive BLBCs. We replicated this observation in mice, showing that TAZ is activated starting from the precancerous stage of BLBC but not ESR^+ luminal cancers. Unlike TAZ's involvement, however, the involvement of YAP1 activation in human BCs has been controversial. Some groups have reported the presence of greater levels of activated YAP1 protein in tumor cells from patients with invasive TNBC (59.9%) compared to invasive ESR^+/PGR^+ (29.7%) or $HER2^+$ (10.8%) cancers (44, 45). This elevation of activated YAP1 also correlated with aggressive tumor behavior and reduced metastasis-free survival. On the other hand, several teams have shown that, compared to normal human breast tissue, YAP1 was not activated in invasive ESR^+/PGR^+, $HER2^+$, or TNBC malignancies (20). In addition, loss of heterozygosity for the chromosomal region containing the *YAP1* gene has been observed in 33 to 43% of invasive BC cases (46, 47), and the *YAP1* promotor is frequently methylated in BC patients (48). We showed here that nuclear YAP1 activation was not increased at either the precancerous or invasive stage of BCs (including BLBCs), and this BLBC formation was not prevented by additional loss of YAP1 in our mutant mice. Thus, we conclude that TAZ, rather than YAP1, is the more important oncogenic effector in BLBC carcinogenesis in mice and humans. We speculate that the studies reporting YAP1 activation in BLBCs may have resulted from a lack of tight YAP1 specificity of the antibodies used in the relevant IHC experiments. Because TAZ and YAP1 are paralogous molecules, these antibodies may have, in fact, recognized activated TAZ.

A previous report demonstrated that overexpression of TAZ in freshly prepared human MECs or normal human MCF10A cells increased the appearance of the basal-like phenotype and that inhibition of TAZ in MCF10A cells led to their luminal differentiation in vitro (49). This group also showed that TAZ-deficient mice exhibited reduced numbers of normal basal cells with an accompanying decrease in mammary gland cellularity. However, when they knocked down YAP1 in MCF10A cells, they did not see a similar alteration to their lineage marker profile (49). Therefore, although it seems that TAZ (but not YAP1) can alter the fate of normal breast epithelial cells, it remains to be clarified whether TAZ activation in luminal BC cells skews their differentiation toward the BLBC type. We have shown in our study that MOB1 loss in luminal cells initiates the formation of luminal BCs that gradually change the profile of their surface markers to that of BLBCs. We also demonstrated that an ESR^+ luminal cancer cell line induced to overexpress TAZ lost its luminal BC phenotype and acquired a BLBC phenotype. Thus, continuous activation of TAZ may skew early-onset luminal BC cells toward the BLBC fate.

ΔNp63 is the major isotype of Tp63 in mammary glands and is highly expressed specifically in normal immature stem/progenitor cells and mature myoepithelial/basal cells (50). ΔNp63 knockdown in primary human breast epithelial cells induces a decrease in basal cell markers and an increase in luminal markers (51), implying that enhanced expression of ΔNp63 in mammary tissues might drive an increase in basal markers and a decrease in luminal markers, just as we observed in our MOB1-deficient mice. It may be that TAZ hyperactivation has downstream effects that lead to excessive ΔNp63 activity, which could partly explain the basal-like phenotype of BCs in our MOB1-deficient mice.

TP53 mutations are more frequent in human invasive BLBCs (88% positive) than in either luminal BCs (26% positive) or HER2-amplified BCs (50% positive) (52). However, we showed here that *TP53* mutation is rare in human BLBCs at the DCIS stage, implying that TP53 inactivation is not an initiating event in BC carcinogenesis. Using our mutant mice, we demonstrated that TP53 inactivation layered on top of Hippo-TAZ activation accelerates tumor progression. These observations suggest that *TP53* mutation is a late event that causes BLBCs to acquire more aggressive features.

In conclusion, our paper has provided genetic evidence that the Hippo-TAZ pathway is a key driver of the onset and progression of BLBCs because this aberrant signaling triggers incipient luminal cell tumors to acquire a BLBC phenotype. Our results further suggest that subsequent *TP53* mutation (possibly induced by the genetic instability caused by altered Hippo-TAZ signaling) confers increased aggressiveness on BLBCs. The Hippo-TAZ pathway thus becomes an appealing molecular target for novel therapies of BLBC. We are now screening various drugs capable of targeting the Hippo-TAZ pathway and employing our mutant mice as a useful tool for their evaluation. Our goal is to identify one or more such drug candidates whose administration could bring concrete benefits to BLBC patients.

Materials and Methods

Mice. Mouse strains used in this study were *PGR-Cre* (27); *Mob1a*$^{flox/flox}$;*Mob1b*$^{-/-}$ (23); *Rosa26-LSL-YFP* reporter (The Jackson Laboratory); *Rosa26-LSL-tdTomato* reporter (The Jackson Laboratory); *Rosa26-CreERT2* (The Jackson Laboratory); *Trp53*$^{flox/flox}$ (The Jackson Laboratory) and *Taz*$^{flox/flox}$ (kindly provided by Dr. J. Wrana, Lunenfeld-Tanenbaum Research Institute). *Yap1*$^{flox/flox}$ mice were generated using *Yap1*$^{flox/flox}$ ES cells from the Knockout Mouse Project Repository. *PGR-Cre* and *Rosa26-CreERT2* mice were of the C57BL/6 background, and *Mob1a*$^{flox/flox}$;*Mob1b*$^{-/-}$ mice were back-crossed to C57BL/6 for more than six generations. Postnatal *Mob1a/b* double homozygous mutant mice (*Rosa26-CreERT2;Mob1a*$^{flox/flox}$;*Mob1b*$^{-/-}$ mice; designated *ro*Mob1 DKO) were generated by administering a single i.p. dose of 1 mg TAM (Toronto Research Chemicals, Toronto, Canada) at 8 to 12 wk of age. Primers used for genotyping PCR are listed in *SI Appendix*, Table S1*A*. All mice were kept in specific pathogen-free facilities at Kobe University.

Mammary Organoid Culture. Organoid culture was performed essentially as previously described (53) using mammary luminal cells that were freshly sorted from *Rosa26-CreERT2;Mob1a*$^{flox/flox}$;*Mob1b*$^{-/-}$ or control mice. These cells were pretreated with 0.5 μM TAM for 2 d, mixed with 20 μL Matrigel (Corning), embedded in prewarmed (37 °C) 48-well plates, and incubated for 15 to 30 min to allow solidification. Plates were then overlaid with DMEM/F12 advanced medium supplemented with Hepes (1:100, GIBCO), L-glutamine (1:100, GIBCO), B27 (1:50, Thermo Fisher), 100 ng/mL A83-01 (Tocris Bioscience), 50 ng/mL EGF (PeproTech) and 10 μM Y-27632 (Sigma-Aldrich) and cultured without TAM for up to 12 d to generate organoids.

Clinical Samples. Randomly selected, surgically obtained human breast DCIS (ESR/PGR-positive [$n = 40$] or negative [$n = 60$]) or IDC (ESR/PGR-positive [$n = 20$] or negative [$n = 30$]) samples that also contained noncancerous tissue were acquired from Hyogo Cancer Center, Kobe City Medical Center General Hospital, or Kyushu University Beppu Hospital. ESR/PGR-positive samples were considered to be luminal BCs. Resected tissues were fixed in formalin and stained with anti-YAP1 (Sigma-Aldrich), anti-TAZ (Sigma-Aldrich), anti-KRT5 (DAKO), anti-ESR (DAKO), or anti-p53 (DO-7, Santa Cruz) antibodies (*SI Appendix*, Table S2) using a standard protocol. UDH and ADH were histologically defined in regions adjacent to DCIS in the same tissue sections. Among ESR/PGR-negative samples (DCIS or IDC), KRT5-positive (50% or greater positive staining) samples were

considered to be BLBCs. Scoring of YAP1 and TAZ activation was conducted either as described in Fig. 5*A* or by ImageJ analysis of 3,3′-diaminobenzidine (DAB) staining measured in arbitrary units (AUs). Cancer cells showing 10% or greater strong positive nuclear p53 staining, or a complete absence of nuclear and cytoplasmic p53 staining, were considered to bear TP53 alterations.

Study Approval. Animal experiments were approved by the Kobe University Animal Experiment Committee (P60602-R8, P170603), and animal care was conducted in accordance with institutional guidelines. The full clinical study protocol was approved by the ethics committees of Kobe University Hospital (No. B210093); Hyogo Cancer Center (No. R-922); Kobe City Medical Center General Hospital (No. 21102); and Kyushu University (No. 21031-00). Written informed consent was obtained from all patients whose cancers were analyzed in this study.

Data Availability. All study data are included in the article and/or *SI Appendix*.

ACKNOWLEDGMENTS. We thank H. Togashi, Y. Miyachi, and M. Suzuki (all of Kobe University) for expert technical assistance and critical discussions. We thank J. Wrana (Lunenfeld-Tanenbaum Research Institute) for *Taz*$^{flox/flox}$ mice.

We are grateful for the funding provided by the Japanese Agency for Medical Research and Development (grant number 21cm0106114h0006 to A.S.); the Japanese Society for the Promotion of Science (JSPS KAKENHI, Grant-in-Aid for Scientific Research (A) grant numbers 17H01400 and 21H04806, and Grant-in-Aid for Scientific Research on Innovative Areas grant number 20H04905, all to A.S.); Nanken-Kyoten, Tokyo Medical and Dental University (TMDU to A.S.); and NIH/NICHD (grant number R01: HD042311 to J.P.L.).

Author affiliations: [a]Division of Molecular and Cellular Biology, Kobe University Graduate School of Medicine, Kobe, Hyogo 650-0017, Japan; [b]Division of Hepato-Biliary and Pancreatic Surgery, Kobe University Graduate School of Medicine, Kobe, Hyogo 650-0017, Japan; [c]Department of Pathology, Hyogo Cancer Center, Akashi, Hyogo 673-8558, Japan; [d]Department of Breast Surgery, Hyogo Cancer Center, Akashi, Hyogo 673-8558, Japan; [e]Department of Diagnostic Pathology, Kobe City Medical Center General Hospital, Kobe, Hyogo 650-0047, Japan; [f]Department of Surgery, Kyushu University Beppu Hospital, Beppu, Oita 874-0838, Japan; [g]Department of Pathology and Biological Responses, Nagoya University Graduate School of Medicine, Nagoya, Aichi 466-8550, Japan; [h]Department of Molecular and Cellular Biology, Baylor College of Medicine, Houston, TX 77030; [i]Medical Innovation Center, Kyoto University Graduate School of Medicine, Kyoto, Kyoto 606-8397, Japan; and [j]Department of Developmental and Regenerative Biology, Medical Research Institute, Tokyo Medical and Dental University, Tokyo, Tokyo 113-8510, Japan

1. R. L. Siegel, K. D. Miller, H. E. Fuchs, A. Jemal, Cancer statistics, 2021. *CA Cancer J. Clin.* **71**, 7–33 (2021).
2. M. E. Hammond *et al.*, American Society of Clinical Oncology/College Of American Pathologists guideline recommendations for immunohistochemical testing of estrogen and progesterone receptors in breast cancer. *J. Clin. Oncol.* **28**, 2784–2795 (2010).
3. A. Marra, D. Trapani, G. Viale, C. Criscitiello, G. Curigliano, Practical classification of triple-negative breast cancer: Intratumoral heterogeneity, mechanisms of drug resistance, and novel therapies. *NPJ Breast Cancer* **6**, 54 (2020).
4. G. Molyneux *et al.*, BRCA1 basal-like breast cancers originate from luminal epithelial progenitors and not from basal stem cells. *Cell Stem Cell* **7**, 403–417 (2010).
5. P. Tharmapalan, M. Mahendralingam, H. K. Berman, R. Khokha, Mammary stem cells and progenitors: Targeting the roots of breast cancer for prevention. *EMBO J.* **38**, e100852 (2019).
6. Cancer Genome Atlas Network, Comprehensive molecular portraits of human breast tumours. *Nature* **490**, 61–70 (2012).
7. E. Cerami *et al.*, The cBio Cancer Genomics Portal: An open platform for exploring multidimensional cancer genomics data. *Cancer Discov.* **2**, 401–404 (2012).
8. J. Gao *et al.*, Integrative analysis of complex cancer genomics and clinical profiles using the cBioPortal. *Sci. Signal.* **6**, pl1 (2013).
9. M. R. Swiatnicki, E. R. Andrechek, How to choose a mouse model of breast cancer, a genomic perspective. *J. Mammary Gland Biol. Neoplasia* **24**, 231–243 (2019).
10. X. Liu *et al.*, Somatic loss of BRCA1 and p53 in mice induces mammary tumors with features of human BRCA1-mutated basal-like breast cancer. *Proc. Natl. Acad. Sci. U.S.A.* **104**, 12111–12116 (2007).
11. Z. Jiang *et al.*, Rb deletion in mouse mammary progenitors induces luminal-B or basal-like/EMT tumor subtypes depending on p53 status. *J. Clin. Invest.* **120**, 3296–3309 (2010).
12. J. D. Holland *et al.*, Combined Wnt/β-catenin, Met, and CXCL12/CXCR4 signals characterize basal breast cancer and predict disease outcome. *Cell Rep.* **5**, 1214–1227 (2013).
13. M. Nishio *et al.*, Hippo vs. Crab: Tissue-specific functions of the mammalian Hippo pathway. *Genes Cells* **22**, 6–31 (2017).
14. K. Nakatani *et al.*, Targeting the Hippo signalling pathway for cancer treatment. *J. Biochem.* **161**, 237–244 (2017).
15. M. Bartucci *et al.*, TAZ is required for metastatic activity and chemoresistance of breast cancer stem cells. *Oncogene* **34**, 681–690 (2015).
16. Q. Y. Lei *et al.*, TAZ promotes cell proliferation and epithelial-mesenchymal transition and is inhibited by the hippo pathway. *Mol. Cell. Biol.* **28**, 2426–2436 (2008).
17. Q. Chen *et al.*, A temporal requirement for Hippo signaling in mammary gland differentiation, growth, and tumorigenesis. *Genes Dev.* **28**, 432–437 (2014).
18. K. E. Denson *et al.*, The Hippo signaling transducer TAZ regulates mammary gland morphogenesis and carcinogen-induced mammary tumorigenesis. *Sci. Rep.* **8**, 6449 (2018).
19. L. Cao, P. L. Sun, M. Yao, M. Jia, H. Gao, Expression of YES-associated protein (YAP) and its clinical significance in breast cancer tissues. *Hum. Pathol.* **68**, 166–174 (2017).
20. Y. Jaramillo-Rodríguez, R. M. Cerda-Flores, R. Ruiz-Ramos, F. C. López-Márquez, A. L. Calderón-Garcidueñas, YAP expression in normal and neoplastic breast tissue: An immunohistochemical study. *Arch. Med. Res.* **45**, 223–228 (2014).
21. J. Díaz-Martín *et al.*, Nuclear TAZ expression associates with the triple-negative phenotype in breast cancer. *Endocr. Relat. Cancer* **22**, 443–454 (2015).
22. Y. W. Li *et al.*, Characterization of TAZ domains important for the induction of breast cancer stem cell properties and tumorigenesis. *Cell Cycle* **14**, 146–156 (2015).
23. M. Nishio *et al.*, Cancer susceptibility and embryonic lethality in Mob1a/1b double-mutant mice. *J. Clin. Invest.* **122**, 4505–4518 (2012).
24. A. Ventura *et al.*, Restoration of p53 function leads to tumour regression in vivo. *Nature* **445**, 661–665 (2007).
25. H. Omori *et al.*, YAP1 is a potent driver of the onset and progression of oral squamous cell carcinoma. *Sci. Adv.* **6**, eaay3324 (2020).
26. Y. Miyachi *et al.*, TAZ inhibits acinar cell differentiation but promotes immature ductal cell proliferation in adult mouse salivary glands. *Genes Cells* **26**, 714–726 (2021).
27. S. M. Soyal *et al.*, Cre-mediated recombination in cell lineages that express the progesterone receptor. *Genesis* **41**, 58–66 (2005).
28. P. M. Ismail, J. Li, F. J. DeMayo, B. W. O'Malley, J. P. Lydon, A novel LacZ reporter mouse reveals complex regulation of the progesterone receptor promoter during mammary gland development. *Mol. Endocrinol.* **16**, 2475–2489 (2002).
29. A. J. Jorgenson *et al.*, TAZ activation drives fibroblast spheroid growth, expression of profibrotic paracrine signals, and context-dependent ECM gene expression. *Am. J. Physiol. Cell Physiol.* **312**, C277–C285 (2017).
30. T. Hashimoto *et al.*, p53 null mutations undetected by immunohistochemical staining predict a poor outcome with early-stage non-small cell lung carcinomas. *Cancer Res.* **59**, 5572–5577 (1999).
31. Z. Wang *et al.*, Analysis of CK5/6 and EGFR and its effect on prognosis of triple negative breast cancer. *Front. Oncol.* **10**, 575317 (2021).
32. Z. Shu *et al.*, A functional interaction between Hippo-YAP signalling and SREBPs mediates hepatic steatosis in diabetic mice. *J. Cell. Mol. Med.* **23**, 3616–3628 (2019).
33. X. Zhou *et al.*, Estrogen regulates Hippo signaling via GPER in breast cancer. *J. Clin. Invest.* **125**, 2123–2135 (2015).
34. Y. Zhao, W. Zhou, L. Xue, W. Zhang, Q. Zhan, Nicotine activates YAP1 through nAChRs mediated signaling in esophageal squamous cell cancer (ESCC). *PLoS One* **9**, e90836 (2014).
35. R. Fan, N. G. Kim, B. M. Gumbiner, Regulation of Hippo pathway by mitogenic growth factors via phosphoinositide 3-kinase and phosphoinositide-dependent kinase-1. *Proc. Natl. Acad. Sci. U.S.A.* **110**, 2569–2574 (2013).
36. L. Xiang *et al.*, HIF-1α and TAZ serve as reciprocal co-activators in human breast cancer cells. *Oncotarget* **6**, 11768–11778 (2015).
37. H. W. Park *et al.*, Alternative Wnt signaling activates YAP/TAZ. *Cell* **162**, 780–794 (2015).
38. S. Di Agostino *et al.*, YAP enhances the pro-proliferative transcriptional activity of mutant p53 proteins. *EMBO Rep.* **17**, 188–201 (2016).
39. Y. Aylon *et al.*, A positive feedback loop between the p53 and Lats2 tumor suppressors prevents tetraploidization. *Genes Dev.* **20**, 2687–2700 (2006).
40. A. Britschgi *et al.*, The Hippo kinases LATS1 and 2 control human breast cell fate via crosstalk with ERα. *Nature* **541**, 541–545 (2017).
41. N. Yabuta, S. Mukai, N. Okada, Y. Aylon, H. Nojima, The tumor suppressor Lats2 is pivotal in Aurora A and Aurora B signaling during mitosis. *Cell Cycle* **10**, 2724–2736 (2011).
42. K. Masuda *et al.*, LATS1 and LATS2 phosphorylate CDC26 to modulate assembly of the tetratricopeptide repeat subcomplex of APC/C. *PLoS One* **10**, e0118662 (2015).
43. N. Furth *et al.*, Down-regulation of LATS kinases alters p53 to promote cell migration. *Genes Dev.* **29**, 2325–2330 (2015).
44. Y. J. Cha *et al.*, High nuclear expression of yes-associated protein 1 correlates with metastasis in patients with breast cancer. *Front. Oncol.* **11**, 609743 (2021).
45. N. Ding *et al.*, Yes-associated protein expression in paired primary and local recurrent breast cancer and its clinical significance. *Curr. Probl. Cancer* **43**, 429–437 (2019).
46. M. Yuan *et al.*, Yes-associated protein (YAP) functions as a tumor suppressor in breast. *Cell Death Differ.* **15**, 1752–1759 (2008).
47. J. Gudmundsson *et al.*, Loss of heterozygosity at chromosome 11 in breast cancer: Association of prognostic factors with genetic alterations. *Br. J. Cancer* **72**, 696–701 (1995).
48. S. A. S. Real *et al.*, Aberrant promoter methylation of YAP gene and its subsequent downregulation in Indian breast cancer patients. *BMC Cancer* **18**, 711 (2018).
49. A. Skibinski *et al.*, The Hippo transducer TAZ interacts with the SWI/SNF complex to regulate breast epithelial lineage commitment. *Cell Rep.* **6**, 1059–1072 (2014).
50. V. Gatti *et al.*, p63 at the crossroads between stemness and metastasis in breast cancer. *Int. J. Mol. Sci.* **20**, E2683 (2019).
51. O. Yalcin-Ozuysal *et al.*, Antagonistic roles of Notch and p63 in controlling mammary epithelial cell fates. *Cell Death Differ.* **17**, 1600–1612 (2010).
52. P. Bertheau *et al.*, p53 in breast cancer subtypes and new insights into response to chemotherapy. *Breast* **22** (suppl. 2), S27–S29 (2013).
53. T. Jardé *et al.*, Wnt and Neuregulin1/ErbB signalling extends 3D culture of hormone responsive mammary organoids. *Nat. Commun.* **7**, 13207 (2016).